Preliminary design of rowing simulator for in-door skill training

Antonio Frisoli, Emanuele Ruffaldi, Leonardo Bagnoli, Alessandro Filippeschi, Carlo Alberto Avizzano, Federico Vanni, Massimo Bergamasco
PERCRO, Scuola Superiore Sant'Anna, Pisa-Italy

ABSTRACT

In this paper we report on the preliminary design of a rowing simulator to be integrated in a VR sport training system for rowing. The proposed simulator aims at bringing in an indoor location the specific features and situations of outdoor rowing, by means of an enhanced Virtual Environment (VE) that combines visual, haptic, acoustic flows to proprio- and exteroception of user status. This paper describes the experimental activities carried out on in-door rowing to characterize the main features of the stroke gesture, the design and analytical study of a fluidodynamic dissipator for force rendering and an overview of graphic simulation and of the overall system architecture.

Categories and Subject Descriptors

H.5.2 [**Information Interfaces and Presentation**]: Haptic I/O; I.2.9 [**Artificial Intelligence**]: Robotics

Keywords

Haptics, Rowing simulator, Skill transfer

1. INTRODUCTION

The rowing simulator presented in this work aims at bringing in an indoor location the specific features and situations of outdoor rowing, by means of an enhanced Virtual Environment (VE) that combines visual, haptic, acoustic flows to proprio- and exteroception of user status. The scope of the simulator is to focus on the preparation of professional athletes (e.g. in rowing federations); however, also possible general fitness applications will be taken into consideration. The VE presented in this work has some similarities with the virtual kayak demonstrator [1], although there are fundamental differences in the haptic interfaces and in the objectives of the project. This work is focused on sport training with measurement of performance while [1] is oriented on entertainment and uses a tendon haptic interface ([2]) that has not been designed for training. Rowing is an Olympic discipline and the number of rowers can be 1, 2, 4 or 8. There are two kinds of rowing:

- Sweep rowing, where each rower has one oar, held in both hands.
- Sculling, where each rower has two oars (one in each hand). The oar in the rowerŠs right hand extends to the port (the left side of the boat), while the oar in his/her left hand extends to starboard (the right side).

The rowing simulator presented in this paper is characterized by three elements. The human, the robotic interface and the visualization system. The role of the visualization system is to provide an immersive experience of the virtual rowing activity that is capable to keep the user focused, and at the same time to provide him indications of its current performance and suggestions for improving its pose.

Most of the considerations taken from coaching philosophy and technical training perspective are extracted from "Italian rowing foundation" [3], a handbook distributed from the Italian Federation of Rowing (FIC) to its subscribed athletes. Other information more specifically related to rowing mechanics and physiology are retrieved from some scientific papers. The privileged perspective is that tied to rowing training and therefore several works, for example as those related to rowing applications in rehabilitation, are not considered here. In rowing, oars are used to propel the boat using as sole means athletes muscular effort and the goal of competitive rowing is to cover the racing distance in the minimum allowed time lapse. Except for special categories and racing codes, rowing competitions are performed on a 2000 m distance in a straight line. Such set distance is covered in a time interval lasting between 5 and 9 minutes, depending on the boat type and on the racing conditions. High energetic potential is not enough for a professional rower, and in order to get a successful performance, an expert athlete has to master several further abilities. Among the most crucial ones we find:

- Optimum anaerobic capacity
- Excellent aerobic capacity
- Efficient gesture, with a high biomechanical efficiency
- Ability to manage own energy even when he/she acts expressing high powers and stroke rates

HAS 2008, February 11-14, Quebec, Canada

DOI 10.4108/ICST.AMBISYS2008.2911

- Ability to perform correct movements while carrying out specific additional tasks aimed at overcoming sudden difficulties arisen during a race.

The rowing technique for beginners relevantly differs from the competitive technique, mainly due to the boat speed and the exerted forces, which are lower for beginners and thus induce them to make mistakes. The complexity of the rowing gesture has motivated several biomechanics and sport sciences studies, aimed at understanding the conditions that maximize the stroke efficiency and make athletes more competitive [3, 4]. Moreover the need of a good coordination and the involvement of several muscles has also led to researches on the benefical effect of rowing on health [5, 6], and also - in reason of the intensity and impulsive nature of the forces exerted during the stroke - on the study of damages induced by an uncorrect execution of the stroke gesture [7].

Figure 1: Attack phase in double rowing

2. WHAT IS THE STROKE ?

Rowing is a sport where the athlete moves the ship through one or a couple of oars, by repeating with cyclicity the gesture of *stroke*. During each stroke muscles of legs, back and arms are involved. The sequence of movement is complex enough to require a high degree of coordination. The stroke is defined as the sequence of movements to reach high performances over the race distance, in an efficient way [3]. The stroke can be divided in four phases, that are executed in succession by the athlete:

Catch As the stroke begins, the rower is somewhat coiled forward on the sliding seat, with knees bent, arms outstretched. At the catch, the rower raises the hands to place the oar blade vertically into the water.

Drive At the beginning of the drive, the body position remains the same-the legs do all the work. Then as the upper boy begins to uncoil, the arms begin their work drawing the oar blades through the water. Continuing the drive, the rower moves his hands quickly into his body, which by this time is in a layback position-about the same angle as sitting in a comfortable living room chair.

Finish During the finish the oar handle is lowered, drawing the oar blade out of the water. At the same time, the rower feathers the oar-turns the oar handle-so that the oar blade changes from a vertical position to a horizontal one.

Recovery The oar remains out of the water as the rower begins recovery by moving his hands away from the body and past his knees. The body follows the hands and the sliding seat moves forward, with help from the feet and hips, until the knees are fully bent; the rower is ready to raise his hands for the next catch.

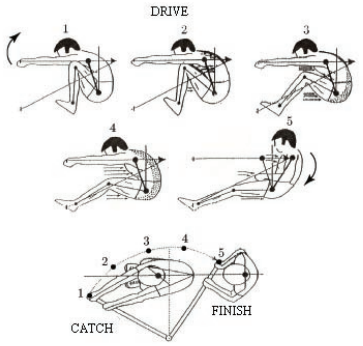

Figure 2: Phase of rowing during one stroke

Experimental measurements of force during stroke reveal the profile shown in figure 3.

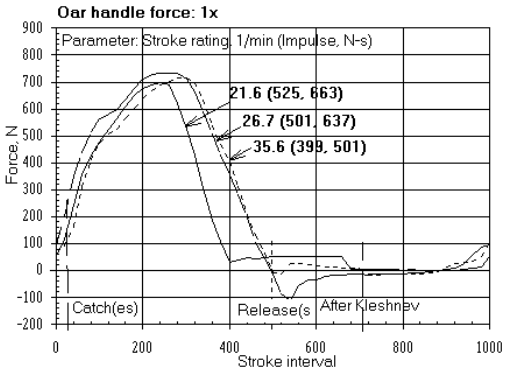

Figure 3: Measured forces in out-door conditions during stroke at the level of handle.

3. EXPERIMENTAL IN-DOOR MEASUREMENT OF ROWING

In order to characterize the force and movement profile during the stroke, some experimental data were acquired from in-door measurements. Experimental in-door activities were conducted by equipping with a load cell one Indoor Rower Model D CONCEPT2 ® and by using a VICON camera system for the motion tracking, as shown in figure 4. The CONCEPT2 ® consists of a flywheel that is mechanically attached to a transmission chain and is moved by the athlete through an handle. A mechanical torsion spring and a fan are mounted in series with the flywheel in order to respectively exert a recalling force during the recovery phase and a viscous resistance force simulating the water drag force. Moreover a free wheel mounted in the overall assembly within the transmission line guarantees that the flywheel is connected to the transmission chain only during the drive phase. Although the system has only 1 degree of freedom,

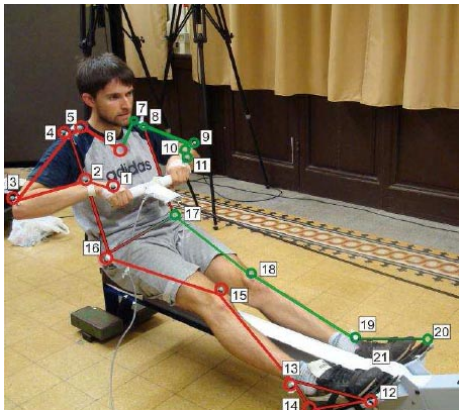

Figure 4: The picture shows the Indoor Rower Model D Concept2 ® with a location of the markers

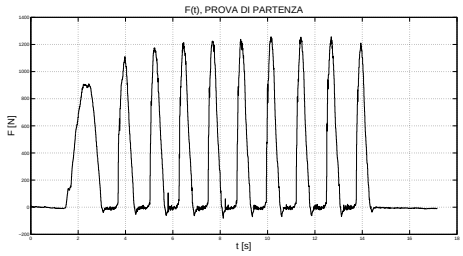

Figure 5: $F(t)$ during the start phase, with a increase of force

and so the kinematics of rowing is highly simplified, this system is widely used for rowing training. Eight cameras and fourteen markes have been used to acquire 12 different type of strokes, different for the frequency, velocity execution and regulations on the adopted indoor rower machine.

In figure 6 we report a plot with the position of wrists and hips, where the different phases of stroke are evidenced. The synchronization between motion and force in real time must be precise. For this reason, the Analog module contained in the VICON system was used to achieve the best possible results in terms of synchronization and accuracy. This analog module is composed of 64 channels with a 16-bits resolution range and a sampling rate of 189KHz. These specifications guarantee a high measuring quality of the force sensor. The force sensor used in these tests was an S-Type load cell Tedea-Huntleigh with a load capacity between 50-100Kg. It was placed between the bar and the chain of the indoor rower, to obtain the force that was applied for the athlete during the performance of the movement.

4. CHARACTERIZATION AND DYNAMIC MODEL OF THE CONCEPT2 ® DISSIPATOR

The maximum condition of overload from experimental measuremens is a force at the level of the handle of 1390 N with a frequency of $n = 46$ strokes / minute. This would require an equivalent torque at the oarlock of $\boxed{C_{zs} = 1.59 \cdot 10^3\,\mathrm{Nm}}$.

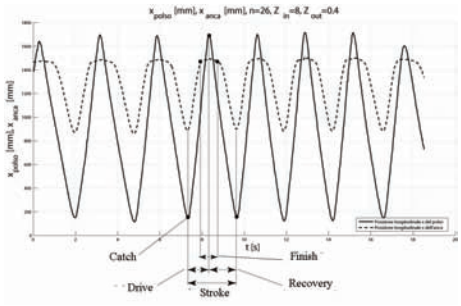

Figure 6: Wrists and hips positions during rowing

Studies conducted on the resistance to forward motion of the boat have shown that the resistance forces are roughly proportional to the square of velocity between boat and water surface, so that a fluidodynamic dissipator with quadratic damping could represent a good approximation of it. This resistance force is generated with good approximation by the Flywheel dissipator that equips the Indoor Rower Model D CONCEPT2 ®. A numerical model of the Flywheel dissipator has been analytically derived and compared with experimental data. A general model for the dissipator includes the effect of a inertia $C_i(t) = -I\ddot{\theta}$, fluidodynamic resistance torque $C_f(t)$, elastic torque $C_e(t) = -k\theta$ due to the torsion spring mounted on the wheel axis to exert the recalling force. The motor force $F(t)$ generated by the athlete, that is transmitted through the transmission chain to the Flywheel, is so given by

$$F\frac{d_m}{2} - I\ddot{\theta} - k\theta + C_f = 0. \tag{1}$$

where d_m is the radius of the pinion gear. The inertia and elastic terms have been computed on the basis of the geometry of the flywheel, while the computation of the fluidodynamic resistance torque requires the solution of an algebraic equation according to a fluidodynamic model.

4.1 Fluidodynamic model of blading

According to fluidodynamics theory, the dissipator can be treated as a centrifugal fan with forward-curved blades, according to the scheme reported in figure 7. By making use of Eulerian theory, we can derive a simple model of the dissipator. However the following hypotheses should hold:

1. *Monodimensionality*: the velocity vector is constant on the blade section;
2. *Permanent condition*: fluid properties and conditions do not change over time.

Clearly the last condition is a strong assumption, due to the pulsating working condition of the machine, so the numerical model will be checked against experimental measurements. According to the Eulerian model, we can easily carry out an energetic balance:

$$\ell = u_2 c_{t2} - u_1 c_{t1}, \tag{2}$$

where ℓ is *virtual work per mass unit* made by the fluid and u_i , c_{ti} are respectively the *tangential velocities* of the blading and the *tangential components of the absolute velocity*

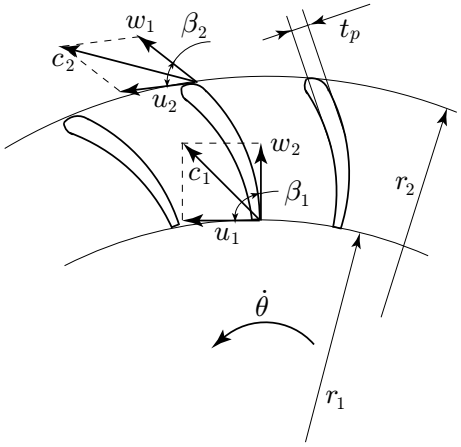

Figure 7: Blading geometry

of incoming ($i = 1$) and outgoing ($i = 2$) flow. According to the velocity triangles shown in Fig. 7 we have:

$$\vec{c} = \vec{u} + \vec{w} \qquad \text{e} \qquad c_{ti} = u_i + w_i \cos\beta_i. \tag{3}$$

So combining the equations Eq. 2 and Eq. 3 we obtain

$$\ell = u_2^2 - u_1^2 + u_2 w_2 \cos\beta_2 - u_1 w_1 \cos\beta_1. \tag{4}$$

As a second hypothesis, we assumed in our model that the fluid is irrepressible, that normally holds for Mach numbers lower than 0.3. If we call Q the *volume flow* of fluid through the blading, c_{mi} the radial components of the fluid absolute velocity, and S_i the net surfaces the fluid goes through, we have

$$Q = c_{m1} S_1 = c_{m2} S_2 \quad \text{ovvero} \quad Q = w_1 \sin\beta_1 S_1 = w_2 \sin\beta_2 S_2. \tag{5}$$

Then substituting the w_i of Eq. 5 in Eq. 4, we have

$$\ell = u_2^2 - u_1^2 + \frac{Q}{S_2} u_2 \cot\beta_2 - \frac{Q}{S_1} u_1 \cot\beta_1. \tag{6}$$

Then since,

$$u_i = \dot{\theta} r_i \qquad \text{e} \qquad W = \rho Q \ell, \tag{7}$$

where W is the *ideal power* given to the fluid and ρ its density, we have

$$W = \rho Q \dot{\theta}^2 (r_2^2 - r_1^2) + \rho Q^2 \dot{\theta} \Big(\frac{r_2}{S_2} \cot\beta_2 - \frac{r_1}{S_1} \cot\beta_1 \Big). \tag{8}$$

So we have obtained a first expression for the power $W(Q, \dot{\theta})$ as a function of flow Q.

4.2 Model of fluidodynamic losses

A second expression for the power $W(Q)$ can be obtained by solving for the pressure drop due to head loss, according to the model of the dissipator as a pipe shown in Fig. 8, with a lumped modeling of flow losses. We can write the Bernoulli's

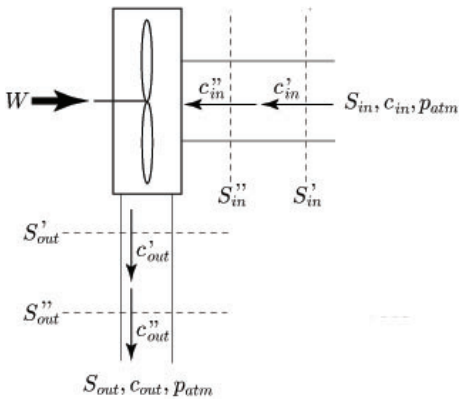

Figure 8: Scheme of head loss within the dissipator

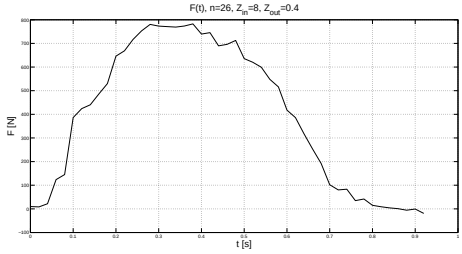

Figure 9: Plot of $F(t)$ during Δt_{forc}

equation in the following form, where all the losses have been modeled through constant coefficients to be determined according to the geometry of pipes and gratings:

$$W = \rho Q \ell = \frac{\rho Q^3}{2} \Big(\frac{1}{S_{out}^2} - \frac{1}{S_{in}^2} + \frac{k'_{in}}{S'^2_{in}} + \frac{k''_{in}}{S''^2_{in}} + \frac{k'_{out}}{S'^2_{out}} + \frac{k''_{out}}{S''^2_{out}} \Big). \tag{9}$$

4.3 Fluidodynamic resistance

By equalling Eq. 8 and 9, we obtain an algebraic equation of second order in the unknown Q:

$$AQ^2 + BQ + C = 0, \tag{10}$$

that can be solved algebrically.

5. EXPERIMENTAL VALIDATION OF THE DISSIPATOR MODEL

The analytical model of the dissipator can be experimentally verified. Due to the higher sampling frequency of acquisition of force measurements, a dynamic inverse approach has been followed to reconstruct the position data from force data through the analytical model of the dissipator. Fig. 9 shows the force plot through the load cell during the phase in which the *free wheel* mounted on the rotor is engaged in gear. This time interval is denoted as Δt_{forc}. For a given number n of strokes per minute, the period for a full stroke is given by

$$T = \frac{60}{n} \tag{11}$$

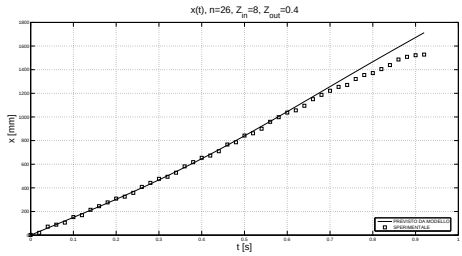

Figure 10: Comparison of wrist position $x(t)$ experimentally measured and predicte by the analytical model for $\Delta t_{lib} < t \leq T$

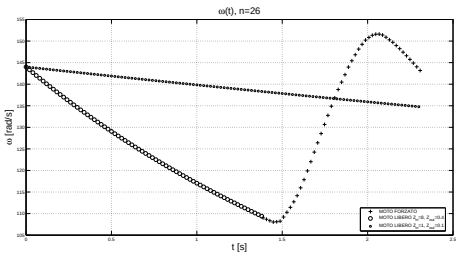

Figure 11: Plot of angular velocity $\omega(t)$ for two different levels of partialization of incoming inflow

When the free wheel is not engaged, the rotor dynamics is free, and so we can assume that the rotor is under free dynamic conditions for

$$0 \leq t \leq \Delta t_{lib} \qquad \text{con} \qquad \Delta t_{lib} = T - \Delta t_{forc} \tag{12}$$

and in force dynamic conditions, with the free wheel engaged, for:

$$\Delta t_{lib} < t \leq T. \tag{13}$$

In the free dynamics condition, the rotor will be slowed down according to the equation

$$I\ddot{\theta} + c_{quad}\dot{\theta}^2 + c_{visc}\dot{\theta} + c_{cost} = 0, \tag{14}$$

The differential equation is not ordinary, and it has been solved numerically with forward-Euler integration method.

The forced dynamics equation is given by

$$\boxed{I\ddot{\theta} + c_{quad}\dot{\theta}^2 + c_{visc}\dot{\theta} + k\theta + c_{cost} = F\frac{d_m}{2}.} \tag{15}$$

with the initial conditions

$$\theta(\Delta t_{lib}) = 0 \quad \text{e} \quad \dot{\theta}(\Delta t_{lib}) = \omega(\Delta t_{lib}), \tag{16}$$

that means that the initial velocity of the forced dynamics coincides with final velocity of the free dynamics condition. In order to find the correct value if the initial velocity, that satisfies the periodicity condition

$$\omega_0 = \dot{\theta}(T). \tag{17}$$

an iterative procedure has been adopted, adopting a starting guess value for ω_0, and then converging iteratively to the final value. The comparison with the experimental kinematic data can be made through the plot of the longitudinal wrist position, during the interval $\Delta t_{lib} < t \leq T$, and it is shown in figure Fig. 10.

The experimental data fit well with the motion predicted by the model. In Fig. 11, we report the plot of angular velocity, as predicted by the model, for ω per $0 \leq t \leq T$ and in agreement with experimental data. In the same figure, it is also shown how a partialization of air inflow, superimposed over the evolution without partialization, can be used to modify the parameters of the force profile during the stroke exerted by an athlete.

The main effect of the parzialization of airflow (usually obtained through an inflow grating with variable section) is a reduction of the maximum force, that according to figure Fig. 9 is half of the previous value. It can be shown that the partialization represents a way to modulate the maximum force developed by the athlete during the stroke, still preserving the parabolic shape of the experimental force profile observed in Fig. 3. It should be stated more precisely however, that the partialization does not guarantee an absolute reduction of force, since it will depend however on the adaptation of the athlete to the new fluidodynamic parameters and its variation of stroke kinematics. But the computer-controlled partialization of airflow, based on the numerical module herewith presented, constitutes an efficient method to change the force response of the system according to the status of the simulation. This can be easily made by controlling the fan inflow through the aperture of the input grating and represents an intrinsically passive and stable technique to simulate the drag effect of water on the boat, in good agreement with experimental data.

5.1 Summary of results

From the analysis of the dissipator, the athlete stroke in in-door rowing, can be divided into two different phases, according to the status of the free wheel mounted on the rotor.

1. When the free wheel is not engaged, there is a decrease of velocity of the rotor according to its free dynamics determined by the fluidodynamic resistance.
2. When the free wheel is engaged, the athlete transmits the pulling force through the transmission chain, and there is an acceleration of the rotor determined by its forced dynamics

Overall, the contributions to the overall force resistance, are shown in Fig. 12, where the main terms composing the stroke force are given by the fluidodynamic, inertial and elastic contributions, with a predominant role played by the inertial contribution.

6. LAYOUT OF THE SIMULATOR

We decided to adopt in our design a layout employing a double dissipator configuration for each oarlock, to allow rowing on the same simulator with one or two oars. This solution has required a 90° change of motion that has been obtained through angular speed reducers with conic gears followed by co-axial epycicloidal gears. The inversion of the

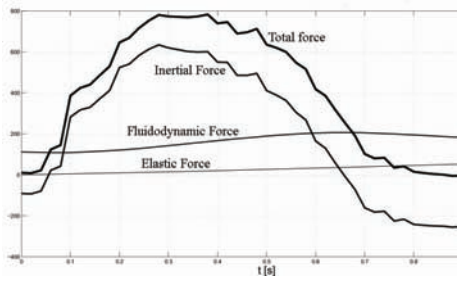

Figure 12: Different component of force resistances

motion, since the dissipator is designed for working only with one sense of rotation, has been solved by an asymmetrical disposition of the two speed reducers as shown in figure 13.

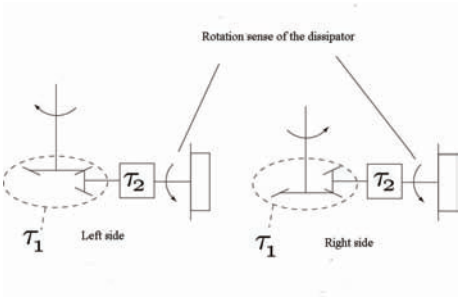

Figure 13: Dissipator layout with axes orthogonal to the oarloack axis

In Fig. 14 it is shown a 3D CAD model of the simulator with the final layout, while in Fig. 15 the first prototype of the simulator is shown during the catch phase.

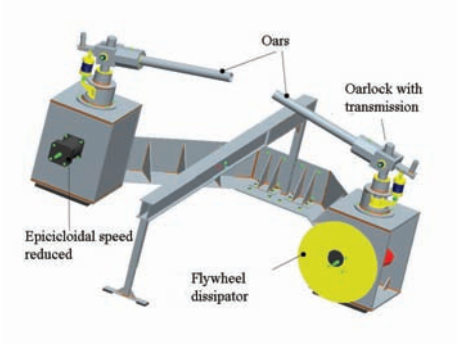

Figure 14: CAD model of the simulator

The mechanical simulator is equipped with encoders for sensing of motion and strain-gauges mounted on the transmission shafts for force sensing, even if the accurate model derived for the dissipator unit allows to estimate indirectly the force response from the acquisition of only kinematic data. The overall architecture of the simulator is shown in figure 16. In front of the mechanical simulator is placed the projection system that shows a Virtual Environment in which the

Figure 15: First prototype of the simulator

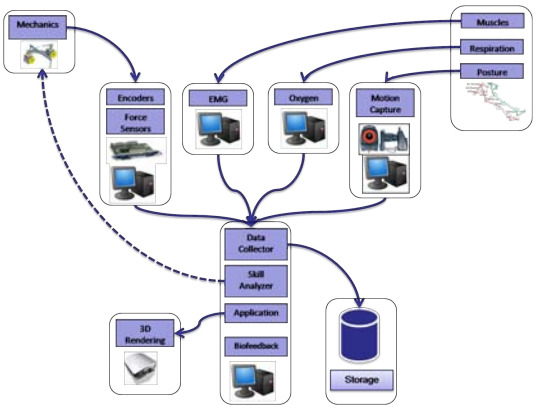

Figure 16: System architecture of the Rowing Simulator, highlighting the sensor and the computational elements

user is immersed and it provides the context in which the rowing exercises takes place. The visualization system has been conceived to be non stereographic because of the additional encumbrance caused by the glasses, and given the fact that there is no specific task for which the stereography is required. During the research phase of the simulator there is an additional system that is used for analyzing the user performance, it is an optical motion tracking system, like the Vicon (OMG, Uk). The information coming from the sensors of the mechanical interface, from the motion capturing and the bio-sensors will be integrated into a machine learning system that analyzes in real-time the performance of the user in terms of single movements and gesture signature. This analysis is based on the construction of model from the recording of good performing users and adapted to the specific characteristics of the user. At every instant of execution, user data are compared against the model for the evaluation of performance indices, shown as biofeedback to the user, and for the generation of visual and audio stimuli, rendered in the VE suggesting corrective actions for the user.

7. VIRTUAL ENVIRONMENT

The training activity can be simulated in a variety of ways depending on the level of the user and the training objectives, in particular it is possible to perform single boat simulations and multiple boat races. The user, placed in front

Figure 17: Layout of the VE

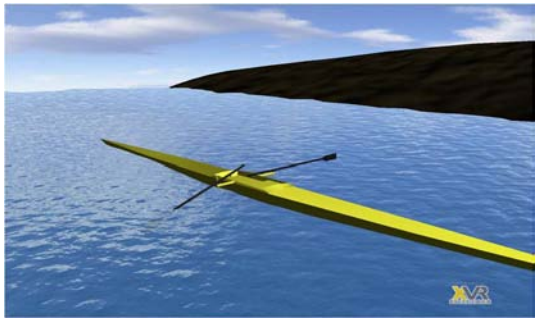

Figure 18: The overall model of the boat and the water

of the visualization screen, sees a representation of its own boat while it moves in the water, with a background environment containing the sides of the river or lake. Because of this point of view the avatar of the user is not displayed while in the case of multiple boats the other avatars are displayed and animated. In Fig. 17 a training activity on the CONCEPT2 ® ergometer integrated the VE is shown. The kinematics of the virtual oars is synchronized with the ergometer handle by means of the flywheel angular velocity signal and of the strokes cadence.

The VE is structured around some fundamental elements: boats, avatars, environment and water, each characterized by a certain level of realism. Because VE simulation does not require a detailed simulation of the hydrodynamics of the boat or the flow of the water around it, the boat and the water have been modeled in terms of graphical visualization. In particular the boat has been geometrically modeled from existing boats without a detailed model of the boat profile or the volumes, in this context is only necessary to make the visualization of the boat realistic, addressing the material properties of the boat itself. If specific dynamic analysis is needed an existing boat could be eventually laser scanned and modeled in detail. The canal in which the simulation takes place has been modeled using a terrain generator tool that allows to easily manage the surface properties and the additional environmental details.

In terms of realism, the water and the sky are the elements that require additional care. During the training task the user is not focused on a specific part of the scene and he

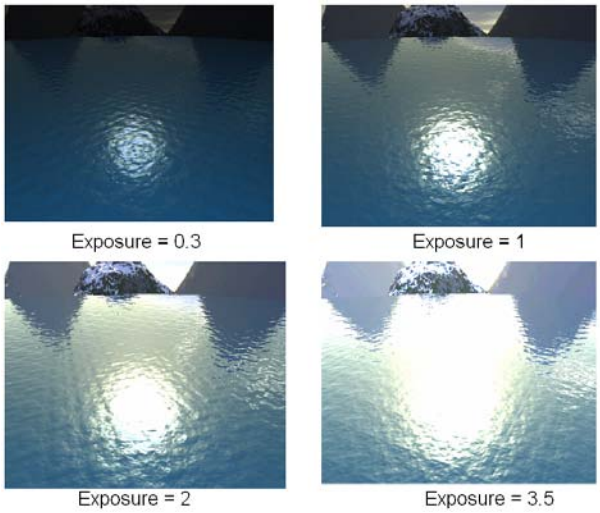

Figure 19: Effect of the exposure parameters with the HDR technique

doesn't look at specific features. Instead the user is highly afftected by the global lighting condition that is generated by the water visualization. The lighting effects the water are more relevant than the physically based simulation [8], and in any case the techniques adopted for the visualization could be integrated with the simulation itself. The water surface has been modeled using a height map that is randomly disturbed for simulating the movements caused by waves and wind. The heigh map is fundamental for the application of the various effects that makes the water look realistic and in particular there are three specific techniques: reflection, refraction and Hight Dynamic Range [9].

The reflection is based on a simplification of the Fresnel equation and it allows to reflect on the water the boat and the background environment, and in particular clouds and sun. The refraction of light under water, based on the Snell equation, affects the display of the bottom of the sea and the display of objects that are under water. Given the assumption of shallow water is sufficient to model the visualization of objects in the water, in particular the oars. The standard display techniques are not sufficient for the visualization of an outside environment like the one described here, there are reflections and highlights that are not represented. The High Dynamic Range (HDR) rendering is a technique that represents the lighting condition of the sky in exponential form, allowing to extend the range of colors coming from the sun. In 19 is shown the effect of the HDR with different parameters of exposure. The overall visualization of the water is completely in real-time thanks to the use of hardware OpenGL Shaders [10].

8. CONCLUSIONS

This paper has presented the preliminary design and overview of a rowing simulator for skill training and analysis of performance in in-door rowing.

9. ACKNOWLEDGEMENTS

This project is being developed within the European IP project SKILLS "Multimodal Interfaces for Capturing and Transfer of Skill" under the contract number IST-2006-035005-SKILLS funded by European Commission.

10. REFERENCES

[1] Yoshinori Dobashi, Makoto Sato, Shoichi Hasegawa, Tsuyoshi Yamamoto, Mitsuaki Kato, and Tomoyuki Nishita. A fluid resistance map method for real-time haptic interaction with fluids. *VRST '06: Proceedings of the ACM symposium on Virtual reality software and technology*, pages 91–99, 2006.

[2] J. Murayama, L. Bougrila, Y. Luo, K. Akahane, S. Hasegawa, B. Hirsbrunner, and M. Sato. SPIDAR G&G: A Two-Handed Haptic Interface for Bimanual VR Interaction. *Proc. EuroHaptics 2004*, pages 138–146, 2004.

[3] G. La Mura. *I Fondamenti del canottaggio italiano*. Centro Tecnico Nazionale Federazione Italiana Canottaggio, 1997.

[4] A. Baudouin and D. Hawkins. Investigation of biomechanical factors affecting rowing performance. *Journal of Biomechanics*, 37(7):969–976, 2004.

[5] R. Davoodi, BJ Andrews, GD Wheeler, and R. Lederer. Development of an indoor rowing machine with manual FES controller for total body exercise in paraplegia. *Neural Systems and Rehabilitation Engineering, IEEE Transactions on [see also IEEE Trans. on Rehabilitation Engineering]*, 10(3):197–203, 2002.

[6] S.E.H. DPhil, A.B.Z. DPhil, and K.H. PhD. Can functional electric stimulation-assisted rowing reproduce a race-winning rowing stroke? *Archives of Physical Medicine and Rehabilitation*, 85(8):1265–1272, 2004.

[7] F. OŠSullivan, J. OŠSullivan, A.M.J. Bull, and A.H. McGregor. Modelling multivariate biomechanical measurements of the spine during a rowing exercise. *Clinical Biomechanics*, 18(6):488–493, 2003.

[8] Lionel Baboud and Xavier Décoret. Realistic water volumes in real-time. In *Eurographics Workshop on Natural Phenomena*. Eurographics, 2006.

[9] S. Premoze and M. Ashikhmin. Rendering Natural Waters. *Computer Graphics Forum*, 20(4):189–199, 2001.

[10] K. Iwasaki, Y. Dobashi, and T. Nishita. A Fast Rendering Method for Refractive and Reflective Caustics Due to Water Surfaces. *Computer Graphics Forum*, 22(3):601–609, 2003.